S.W. Vincent, S.I. Jackson, C. Chiquete, M. Short.
"The Geometric Scaling of IMX-104 Explosive: Detonation Velocity versus Charge Size for Cylindrical Rate Sticks and Slab Tests."
In Proceedings of the 15th International Detonation Symposium, Office of Naval Research, pp. 534-543 (Office of Naval Research, 2015)

The Geometric Scaling of IMX-104 Explosive: Detonation Velocity versus Charge Size for Cylindrical Rate Sticks and Slab Tests

Samuel W. Vincent, Scott I. Jackson, Carlos Chiquete, Mark Short
Shock and Detonation Physics Group
Weapons Experiments Division
Los Alamos National Laboratory
Los Alamos, New Mexico, USA

Abstract. We report detonation size-effect data for IMX-104, a new insensitive explosive formulation composed of RDX, NTO, and DNAN. The size-effect data includes numerically predicted and experimentally measured diameter-effect curves from cylindrical-geometry rate sticks and thickness-effect curves from slab tests. These results are used to determine the geometric scale factor that relates explosive performance in the cylindrical geometry to that of the slab geometry. A Detonation Shock Dynamics calibration curve is also provided for IMX-104 based on the available data.

Introduction

It has long been known that the detonation phase velocity D_0 of a condensed-phase explosive will decrease with increasing flow divergence in the detonation reaction zone[1]. This divergence occurs when post-shock pressures exceed the yield stress of the explosive confiner and results in a radial flow component behind the shock front (Figure 1). The onset of radial expansion ahead of the sonic locus induces curvature of the shock front. As the charge radius R decreases, the relative magnitude of the divergence becomes more significant on the detonation, resulting in a decreased D_0. In cylindrical charges, this velocity decrement with diameter is referred to as a high explosive's diameter effect. In slab charges, it is referred to as the thickness effect. The combined diameter- and thickness-effect curves are referred to here as the size effect.

Comparison of the scaling of the diameter and thickness effect for condensed-phase explosive has recently been a topic of significant interest[3]. Prior comparisons have been made for homogenous liquid explosives[4], heterogenous solid explosives[5], emulsion explosives[6,7], and non-ideal blasting explosives[8]. Early

Approved for unlimited release: LA-UR-14-24800

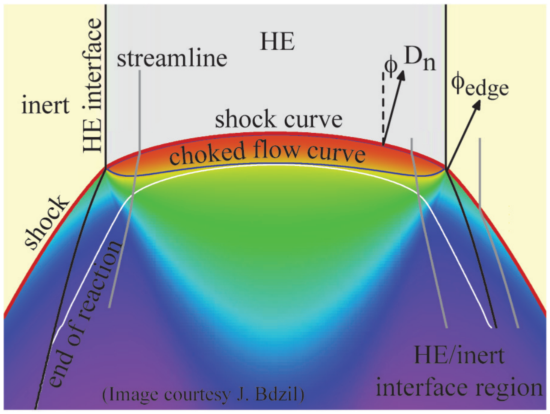

Fig. 1. Divergence-induced detonation curvature from Ref. 2.

work[4–6] measured the critical scale factor, defined as the ratio of the failure radius to failure thickness R_c/R_c in cylindrical- and slab-geometry rate sticks, respectively. More recent studies[7–10] have also measured the steady propagation scale factor, defined as the ratio of radius to thickness at identical detonation velocity $R(D_0)/T(D_0)$.

Researchers have interpreted that curvature-based detonation propagation theories, such as Detonation Shock Dynamics[11] (DSD), predict that all scale factors should be unity[5–8] for explosive propagation where there is a relationship between the normal detonation velocity D_n and the wavefront curvature κ. However, most measured scale factors have not met that expectation, especially for less ideal explosives[4,8,9]. This discrepancy has led some[8,9] to question the applicability of curvature-based propagation theories to non-ideal detonation.

Recently, Jackson and Short[12] used a geometric proof to analytically demonstrate that the scale factor should not, in general, be unity. They[12] also demonstrated that DSD was able to properly predict the diameter effect, thickness effect, and a scale factor that was not unity for PBX 9502 cylindrical rate sticks and slab tests. A subsequent experimental study[10] further validated their analytical effort[12] by measuring average $R(D)/T(D)$ values of 0.98, 0.81, and 0.75 for PBX 9501, PBX 9502, and ANFO, respectively. These results indicated that increasingly non-ideal detonations exhibited scale factors that increasingly deviated from unity.

In the present study, we report the measured scale factors for the new explosive formulation IMX-104. Diameter- and thickness-effect data for this material are presented. The results are set in context to the existing scale factor data from PBX 9501, PBX 9502, and ANFO.

IMX-104 Formulation and Prior Experiment

IMX-104 is an insensitive, melt-castable explosive designed as a direct replacement to the widely used, more sensitive Composition B explosive. Previously referred to as PAX-33 MOD, IMX-104 was recently developed[15] by ARDEC, the U.S. Army Armament Research, Development and Engineering Center and is composed of RDX, NTO, and DNAN. Sensitivity testing has shown this energetic material to have output energy similar to that of Composition B, but with much lower shock and friction sensitivity. Eight cylindrical rate sticks were previously fielded to characterize the diameter effect and D_n–κ relation for IMX-104[13]. Five slab-geometry rate sticks were fielded to measure the thickness effect in this study.

Figure 2 shows the the measured diameter effect on a plot of detonation velocity versus inverse charge radius. The black points are from our prior measurements (Ref. 13 and more recent tests). The red points are from ARDEC's prior work[14]. The curves are generated from Eyring-form[16] fits to different combinations of the cylindrical rate-stick data using the diameter-effect measurements as discussed in Ref. 17.

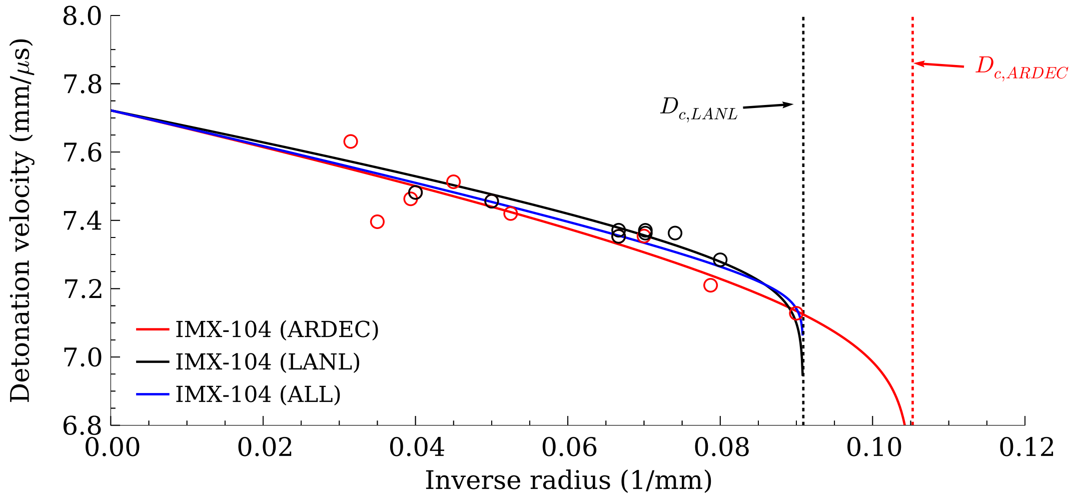

Fig. 2. The diameter-effect curves for IMX-104. Black points are from Ref. 13. Red points are from Ref. 14.

Experimental

The slab test geometry is an unconfined variant of the detonation sandwich test[18] that generates a region of two-dimensional quasi-steady flow for measurement of detonation velocity and front shape. Figure 3 is an image of the 17.5-mm-thick slab test, which consists of consists of a high-aspect-ratio rectangular-cuboid main charge that was boosted by two pieces of PBX 9501 and initiated by two detonation line wave generators[19,20].

Ionization probes, located in the center of the slab, measure the detonation position versus time relationship. As the detonation velocity is steady at the core of this geometry, the slope of a linear fit to the position-time data yields the detonation velocity. Additional details pertaining to the design and operation of the test are discussed in Ref. 10. Front shapes were also measured using the mirror turning technique (discussed in Ref. 21) and illumination via an Argon flash[22].

Slab tests were performed at five thicknesses intended to compare well with the prior cylindrical rate stick data when plotted in size-effect space (detonation velocity versus the inverse charge radius/thickness). The dimensions of each test, resulting detonation velocity, and standard error are listed in Table 1.

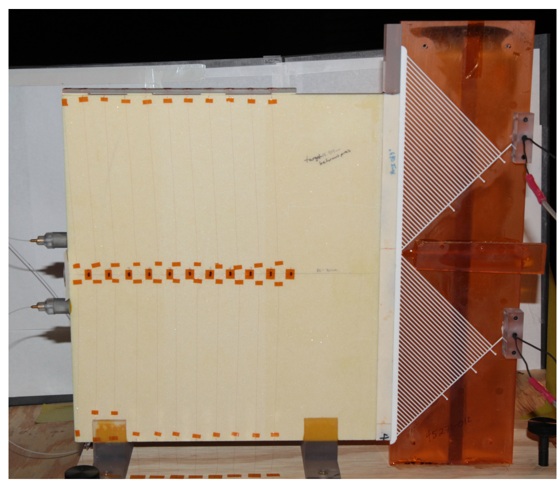

Fig. 3. The slab test geometry.

Front Curvature Analysis

To obtain a representation of the shock front shape in the shock height z versus radius r

Table 1. Slab test thickness t, length L, width w, initial density ρ_0, detonation velocity D_0, and standard error SE.

t mm	L mm	w mm	ρ_0 g/cm^3	D_0 mm/μs	SE mm/μs
9.99	140.0	160.0	1.758	7.157	$\pm$0.004
12.55	175.1	200.0	1.756	7.341	$\pm$0.003
15.06	210.1	240.0	1.751	7.411	$\pm$0.004
17.51	245.1	280.1	1.755	7.472	$\pm$0.002
19.31	270.2	308.8	1.755	7.503	$\pm$0.003

Table 2. Log-form fit parameters with fitted edge angle.

Test #	T (mm)	A_1 (mm)	A_2 (mm)	A_3 (mm)	η	ϕ_e (deg)
8-1850	9.990	1.3371	0.0000	0.0013	0.7527	37.79
8-1846	12.550	1.1142	——	——	0.8166	37.54
8-1847	15.060	1.0367	——	——	0.8449	36.32
8-1848	17.510	1.0904	——	——	0.8593	36.81
8-1849	19.310	0.9491	——	——	0.8977	40.52

plane, a digitized image of the front breakout is produced and reduced according to magnification factors obtained from the axial detonation velocity and included fiducial in the image. To determine a base representation of the crucial normal velocity-curvature relation that involves derivatives of the front, experimental front shapes were fit using the form used discussed in Hill[23]. It is a series function form based on the work of Bdzil[24],

$$z(r) = -\sum_{i=1}^{n} A_i \left[\ln\left(\cos\left(\frac{\pi\eta}{2R_e}r\right)\right)\right]^i, \quad (1)$$

where r is the local radius and the parameters A_i and η are fitting constants such that $0 < \eta < 1$ and $n = 1$ except for the smallest test (8-1850, $T = 9.99$ mm) where it was necessary to use $n = 3$ for fitting the slab front shape data.

The normal velocity D_n and the front curvature κ can then be found from the curvature relations,

$$D_n = \frac{D_0}{\sqrt{1+(z')^2}}, \quad (2a)$$

$$\kappa = \frac{z''}{[1+(z')^2]^{3/2}} + \alpha\frac{z'}{r\sqrt{1+(z')^2}}, \quad (2b)$$

where $z' = dz/dr$, $z'' = d^2z/dr^2$ and α determines whether the underlying test geometry is cylindrical ($\alpha = 1$) or slab ($\alpha = 0$). Use of a twice continuously-differentiable ($\mathcal{C}^2$) analytic function for $z(r)$ yields smooth values of the first and second derivatives ($z'(r)$ and $z''(r)$) and avoids the significant noise that would be generated in the numerical differentiation of the raw wave front data.

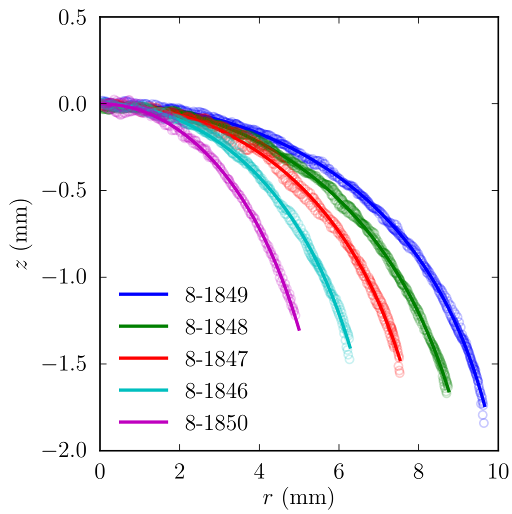

Fig. 4. The produced detonation front shapes for the slab tests in circles. Additionally, log-form fits to the front shapes appear as lines.

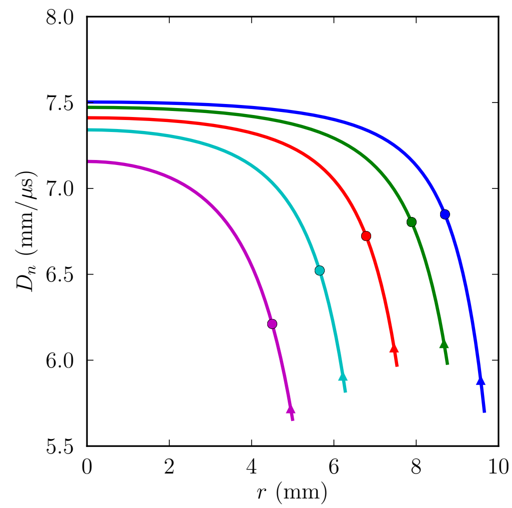

Fig. 5. The variation of the normal detonation velocity D_n vs. r produced from the log-form fits to the front shapes.

The variation of the normal detonation velocity and total curvature κ appear in Figures 5 and 6 for all the tests carried out in this series. The circle and triangle symbols in these series of plots represent the 90% and 99% extent of each detonation front shape. These are parametrically plotted in Figure 7. The central three front shapes overlapped very well when plotted in D_n-κ space, but the largest and smallest tests significantly diverged from the central core.

DSD Calibration

To calibrate an explosive for DSD, a functional form for the D_n–κ relation must be specified and its parameters systematically varied to optimally fit the available experimental data within the calibration procedure. To quantify the quality of a particular fit, a merit function must be defined that incorporates the error in the DSD-calculated detonation velocity and front shapes into a single metric. Here it is defined as

$$\mathcal{M} = w \sum_{i=1,N_{DE}} (F_i(D_{0,i}^{calc} - D_{0,i}^{exp}))^2 + \quad (3)$$

$$(1-w) \sum_{i=1,N_{FS}} E_i \sum_{j=1,N_r^i} ((\mathbf{z}_j^{i,calc} - \mathbf{z}_j^{i,exp}))^2. \quad (4)$$

The merit function is structured into a size effect component and a front shape error component. The scaling factor between the two sets of data is determined by w. In the calibrations described below, $w = 0.999$ (a value close to 1 since there are many more front point error points than size effect velocity error). The optimized parameters or parameterization of the D_n–κ relation is obtained by numerically minimizing the defined multivariable merit function. With this choice, the final shock front error was 10% of the total merit function value. The calibration procedure used here is based on the approach of Bdzil *et al.*[25].

The specific functional form utilized in this

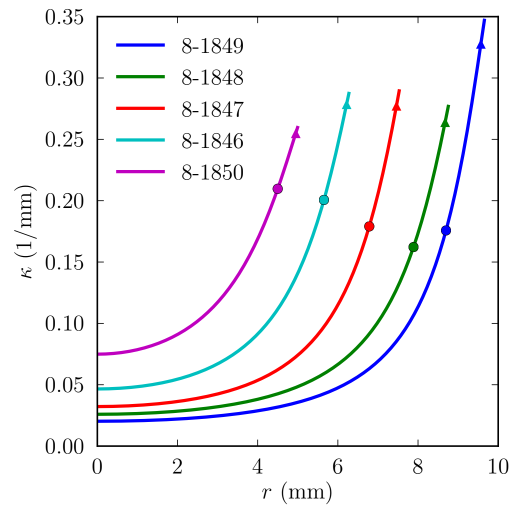

Fig. 6. The variation of the curvature κ vs. r produced from the log-form fits to the front shapes.

work is as follows:

$$\frac{D_n}{D_{CJ}} = 1 - \alpha_1 \kappa \, \frac{1 + \alpha_2 \kappa + \alpha_3 \kappa^2}{1 + \alpha_4 \kappa + \alpha_5 \kappa^2} \tag{5}$$

where the parameters α_i for $i = 1, ..., 5$ were optimized in the minimization of the merit function. The results are plotted in $D_n - \kappa$ space in Figure 8 and the parameters are listed in Table 3.

The comparison of this calibration in terms of the thickness curve appears in Figure 9 and the front shapes appear in Figure 10. The root mean square (RMS) error for the thickness effect data was 32.9 m/s but this is biased by the difficulty of matching the smallest test velocity point (for $T = 9.99$ mm). If one removes that point from consideration, the RMS error becomes 17.2 m/s. The RMS error across all the front shape fits was 0.0638 mm.

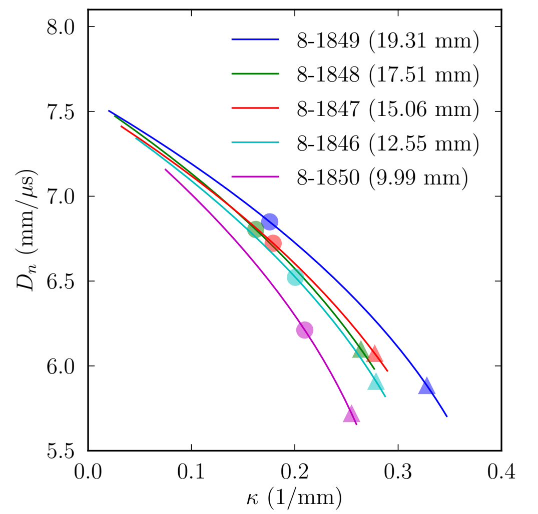

Fig. 7. The experimental D_n-κ data resulting from the log-form fits of the slab front shapes.

DSD calibration prediction of rate-stick data

The series of slab tests shared a consistent bulk or initial density of 1.755 ± 0.002 g/cm^3. As a result the slab-derived fit produced here did not incorporate density dependence in any of the $D_n(\kappa)$ functional form parameters. However, the rate-stick tests for this explosive showed a large range of densities in the explosive segments for each test [13] and the average densities were generally lower than the current slab test average.

Low-density explosive generates less energy release per unit volume and exhibits lower D_0 values. These density-induced velocity variations can overwhelm the size-effect velocity variations and must be corrected for when comparing experiments performed at varying densities. To leading order, density correction is achieved with a linear correction parameter β, such that

$$D_0(\rho_0) = D_0(\rho_{nom}) \times [1 + \beta\,(\rho_0 - \rho_{nom})] \ .$$

Table 3. Optimized fit parameters produced in the calibration of the slab data.

Parameter	Values	Units
D_{CJ}	7.714	mm/μs
α_1	1.491	mm
α_2	0.004	mm
α_3	134.4	mm^2
α_4	9.034	mm
α_5	216.3	mm^2
ϕ_e	35.29	deg

(6)

Parameter β is determined from analysis of the experimental measurements and was determined to be 0.802 from the slab test results.

Figure 11 compares the current calibration prediction of the diameter effect data for a calculation at a nominal density ρ_{nom} of 1.755 g/cm^3 to a "density-corrected" set of the experimental rate-stick velocities (using β = 0.802) to the slab density.

Geometric Scale Factor for IMX-104

The geometric scale factor $R/T(D_0)$ is plotted in Figure 12 for IMX-104 as computed from the DSD calibration curve. The size effect data indicates a steady detonation scale factor $R/T(D_0)$ of approximately 0.82, but that varies with D_0. This measurement is consistent with other explosive measurements [10] and also with theory [12] as it lies below unity. As mentioned, previous measurements [10] indicated average $R(D)/T(D)$ values of 0.98, 0.81, and 0.75 for PBX 9501, PBX 9502, and ANFO, respectively.

Conclusions

Five slab tests were performed with IMX-104 explosive to measure the detonation velocity as a function of charge thickness. The resulting calibration data set consisting of thickness effect and slab front data has been used to characterize the explosive's D_n-κ propagation law necessary for the application of the DSD methodology. In addition, this propagation law was used to generate the corresponding diameter-effect curve. The slab-derived DSD calculation of the diameter effect curve showed some agreement (for the larger tests in that series) with the previously obtained experimental diameter effect data (corrected to account for the higher initial density seen in the slab tests). When combined with prior cylindrical diameter-effect data [13], the slab thickness effect data shows a geometric scale factor that is approximately 0.82, which is consistent with prior measurements [10] for PBX 9501, PBX 9502, and ANFO in that it is below unity [12].

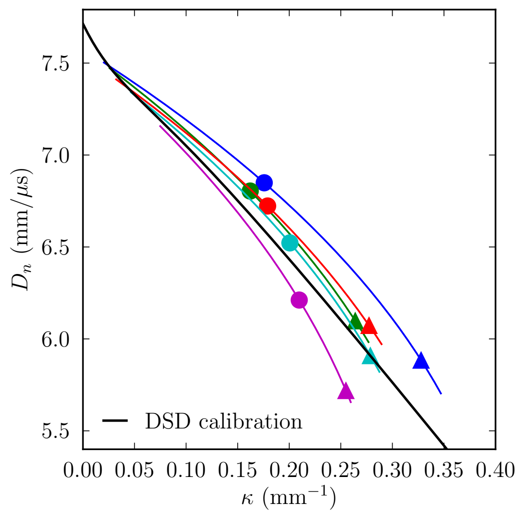

Fig. 8. The experimental D_n-κ data of Figure 7 is compared to the calibrated $D_n(\kappa)$ function (black).

References

1. Jones, H., "A Theory of the Dependence of the Rate of Detonation of Solid Explosives on the Diameter of the Charge," *Provc.*

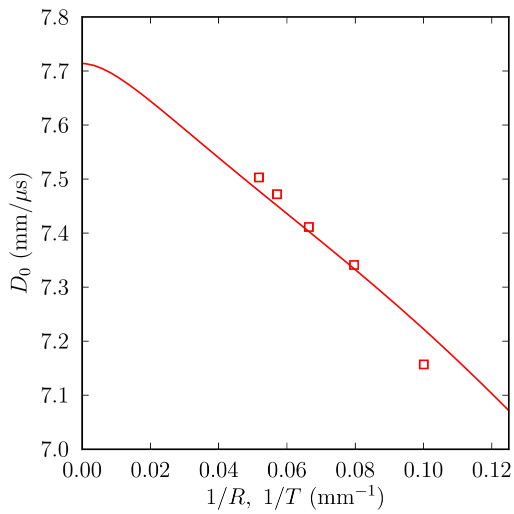

Fig. 9. Comparison of the thickness effect data (points) and DSD calibration calculation (curve).

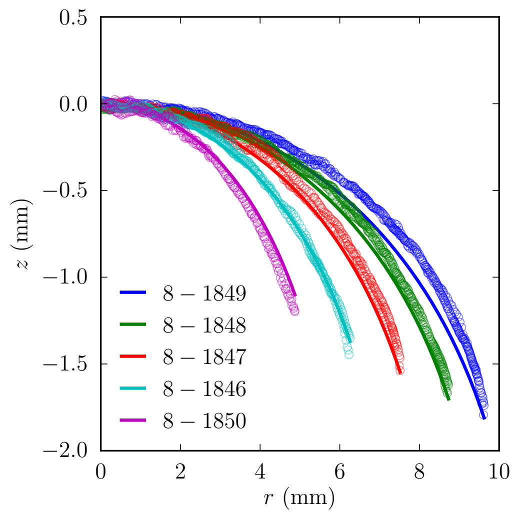

Fig. 10. Comparison of the calculated front shapes and the experimental data.

Royal Soc., Series A, Vol. 1018, pp. 415–426, 1947.

2. Bdzil, J., Aslam, T., Henninger, R. and Quirk, J., "High-Explosives Performance," in "Los Alamos Science," 28, pp. 96–110, Los Alamos National Laboratory, 2003.

3. Petel, O., Mack, D., Higgins, A., Turcotte, R. and Chan, S., "Comparison of the Detonation Failure Mechanism in Homogenous and Heterogenous Explosives," in "Thirteenth (Int.) Detonation Symposium," pp. 2–11, Office of Naval Research, ONR 351-07-01, 2006.

4. Petel, O. and Higgins, A., "Comparison of Failure Thickness and Critical Diameter of Nitromethane," in "Shock Compression of Condensed Matter," pp. 994–997, American Institute of Physics, 2005.

5. Ramsay, J., "Effect of Confinement on Failure in 95 TATB/5 Kel-F," in "Eigth Symposium (Int.) on Detonation," pp. 372–379, Office of Naval Research, 1985.

6. Gois, J., Campos, J., Mendes, R. and Vidal, P., "Effect of Hollow Heterogenities on Nitromethane Detonation," in "Progress in Aeronautics and Astronautics," Vol. 153, pp. 462–480, 1991.

7. Silvestrov, V. V., Plastinin, A. V., Karakhanov, S. M. and Zykov, V. V., "Critical Diameter and Critical Thickness of an Emulsion Explosive," *Combustion, Explosion, and Shock Waves*, Vol. 44, pp. 354–359, 2008.

8. Petel, O., Mack, D., Higgins, A., Turcotte, R. and Chan, S., "Minimum Propagation Diameter and Thickness of High Explosives," *Journal of Loss Prevention in the Process Industries*, Vol. 20, pp. 578–583, 2007.

9. Higgins, A., "Measurement of Detonation Velocity for a Nonideal Heterogenous Explosive in Axisymmetric and

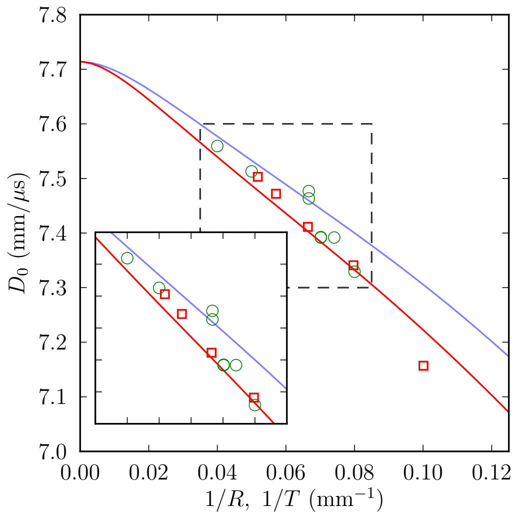

Fig. 11. The calculated thickness curve (—), thickness effect experimental data (□), corrected rate-stick diameter effect data (○), and corresponding prediction from the DSD fit to the slab data (—). Inset shows detail of central region where most of the data is located.

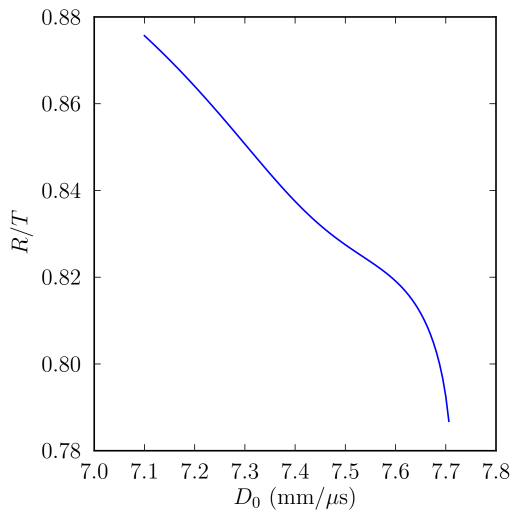

Fig. 12. Evolution of the steady scale factor R/T with D_0.

Two-Dimensional Geometries," in "Shock Compression of Condensed Matter," pp. 193–196, American Institute of Physics, 2009.

10. Jackson, S. and Short, M., "Experimental Measurement of the Scaling of the Diameter- and Thickness-Effect Curves for Ideal, Insensitive, and Non-Ideal Explosives," in "Shock Compression of Condensed Matter - 2013," Vol. 500 of *Journal of Physics: Conference Series*, p. 052020, IOP Science, Bristol, UK, 2013.

11. Bdzil, J. and Stewart, D., "The Dynamics of Detonation in Explosive Systems," *Ann. Rev. Fluid Mech.*, Vol. 39, pp. 263–292, 2007.

12. Jackson, S. and Short, M., "Geometry-Specific Scaling of Detonation Parameters from Front Curvature," in "Proceedings of the 23rd International Colloquium on the Dynamics of Explosions and Reactive Systems," Irvine, CA, July 24–29 2011.

13. Jackson, S., Short, M., Pfau, D. G. and Davis, W. H., "IMX-104 Explosive Rate Stick Tests: Detonation Velocity and Front Shape versus Charge Diameter for DSD Modeling," in "Proceedings of the 44th JANNAF Combustion Meeting," Chemical Propulsion Information Agency, Columbia, MD, 2011.

14. Samuels, P., Zunino, L. and Hu, C., "Qualification of IMX-104," *Technical report*, U.S. Army Armament Research, Development and Engineering Center, Picatinny Arsenal, NJ, 2011.

15. Samuels, P., Singh, S., Vinh, P., DiStasio, A., Zunino, L. and Fishburn, B., "Characterization of PAX-33 MOD," *Technical Report ARMET-TR-09053*, U.S. Army Armament Research, Development and En-

gineering Center, Picatinny Arsenal, NJ, 2009.

16. Cambell, A. and Engelke, R., "The Diameter Effect in High-Density Heterogenous Explosives," in "Proceedings of the 6th International Symposium on Detonation," pp. 642–652, Office of Naval Research, 1976.

17. Chiquete, C., Short, M. and Jackson, S., "Sensitivity and Uncertainty in Detonation Shock Dynamics Parameterization," in "Shock Compression of Condensed Matter - 2013," Vol. Submitted of *AIP Conference Proceedings*, p. In press., American Institute of Physics, Melville, NY, 2013.

18. Hill, L. G. and Aslam, T. D., "The LANL Detonation-Confinement Test: Prototype Development and Sample Results," *AIP Conf. Proc.*, Vol. 706, pp. 847–850, 2004.

19. Jackson, S., Austin, J. and Shepherd, J., "Planar Detonation Wave Initiation in Large-Aspect-Ratio Channels," *AIAA Journal*, Vol. 44, pp. 2422–2425, 2006.

20. Morris, J., Jackson, S. and Hill, L., "A Simple Line Wave Generator Using Commercial Explosives," in "Shock Compression of Condensed Matter - 2009," Vol. 1195 of *AIP Conference Proceedings*, pp. 408–411, American Institute of Physics, Melville, NY, 2009.

21. Rodriguez, G., Sandberg, R. L., McCulloch, Q., Jackson, S. I., Vincent, S. W. and Udd, E., "Chirped Fiber Bragg Grating Detonation Velocity Sensing," *Review of Scientific Instruments*, Vol. 84, p. 015003, 2013.

22. Davis, W., Salyer, T., Jackson, S. and Aslam, T., "Explosive-Driven Shock Waves in Argon," in "Proceedings of the 13th International Detonation Symposium," pp. 1035–1044, Office of Naval Research, 2006.

23. Catanach, R. A. and Hill, L. G., "Diameter Effect Curve and Detonation Front Curvature Measurements for ANFO," in "Shock Compression of Condensed Matter," pp. 906–909, American Institute of Physics, 2001.

24. Bdzil, J. B., "Steady-state two-dimensional detonation," *J. Fluid Mech.*, Vol. 108, pp. 195–226, 1981.

25. Bdzil, J. B., Aslam, T. D., Catanach, R. A., Hill, L. G. and Short, M., "DSD front models: nonideal explosive detonation in ANFO," in "12th Int. Det. Symp.", 2002.